J Mater Sci (2023) 58:11697–11710

Composites & nanocomposites

Ultralight, fire-resistant, lamellar nitrogen-doped graphene aerogels for highly efficient selective organic pollutant cleanup

Ruiqian Zhang[1], Ling Liu[1,*], and Qinghan Meng[1,*]

[1] College of Materials Science and Engineering, Beijing University of Chemical Technology (BUCT), Beijing 100029, China

Received: 24 January 2023
Accepted: 8 July 2023
Published online: 18 July 2023

ABSTRACT

Low-density aerogels have shown great potential as excellent oil–water separation materials in dealing with the growing problem of marine pollution, but they typically suffer from low oil adsorption capacity, complex process flow, expensive raw materials, and poor recyclability. In this paper, inexpensive industrial raw material melamine was introduced into the framework of graphene aerogels, which can be formed into gels (NGAs) in just one step. High-temperature carbonized nitrogen-doped graphene aerogels ($N_{0.5}$CGAs-2) have the advantages of ultralow density, high porosity, repeatable compressibility, hydrophobicity, and excellent adsorption capacity. In addition, depending on the characteristics of the contaminants, $N_{0.5}$CGAs-2 can be selected for different recycling methods and exhibits excellent reusability in cycling. It has a high application value for solving water pollution problems caused by oil spill accidents and chemical spills.

Introduction

Oil spills from oil carriers during transportation have caused severe economic losses and significant damage to local marine ecosystems. Industrial water pollution with dissolved oil or toxic organic reagents also seriously affects the living environment of humans and their health [1, 2]. At present, adsorption, combustion, biodegradation, photolysis, membrane separation [3–7], and other technologies have been applied to oil and water separation of pollutants. Due to its lower cost and operational simplicity, physical adsorption is considered the most appropriate technology for oil pollution treatment. However, achieving high efficiency and low-energy consumption for oil spill cleanup is still a significant challenge. Therefore, it is significant to synthesize a high-performance adsorbent material to adsorb oil and organic solvents. Currently, the commonly used oil-adsorbing adsorbents include three types: natural plant fibres such as cotton, straw, and wood fibres, which are mainly agricultural products

Handling Editor: Jaime Grunlan.

Address correspondence to E-mail: ll@mail.buct.edu.cn; qhmeng@mail.buct.edu.cn

https://doi.org/10.1007/s10853-023-08762-3

that are widely sourced and degradable and have the advantages of economy and environmental protection but have poor adsorption capacity and low efficiency [8–10]. Porous materials such as zeolites, clay, and activated carbon, mainly inorganic materials, are loose, porous, and inexpensive and have good adsorption capacity, but they have poor oil–water selectivity and are difficult to reuse [11, 12]. These traditional adsorbents generally have the disadvantages of relatively low efficiency, insufficient separation capacity, and secondary contamination. Therefore, preparing ideal adsorbents with oil–water selectivity, low cost, simple process, high adsorption capacity, and proper recycling is essential in wastewater treatment [13, 14].

Graphene has a unique single-atomic layer, two-dimensional structure, and large specific surface area, so it is widely used in advanced materials and is considered an ideal precursor for chemical modification and composite assembly [15]. By compounding other materials and controlling the graphene aerogel morphology, low-density, multifunctional, and porous aerogels can be synthesized [16, 17]. For example, graphene/carbon nanotube aerogels have been used as adsorbents for oil–water separation [18], and graphene/COFs (covalent organic frameworks) aerogels have been used as oil adsorbents or supercapacitor-based energy storage devices [15]. Heteroatom doping is a common means of graphene modification. Interestingly, many of the previously reported work, the preparation of nitrogen-doped aerogels was intended to enhance electrochemical performance, but obtained aerogels with excellent physical adsorption properties. Zhao et al. [19] prepared ultralight nitrogen-doped aerogels using small molecules of pyrrole for applications such as oil adsorption, supercapacitors, and catalysts, with up to 600 times the adsorption performance of organic solvents. Wang et al. [20] used polyvinylpyrrolidone to prepare nitrogen-doped aerogels for supercapacitors and oil–water separation. Li et al. prepared [21] that graphene/dopamine aerogels have been used in oil adsorption or high-performance sensors. Nitrogen atom doping of graphene can affect the lattice structure of graphene lamellae, creating better conditions for their adsorption as well as catalytic properties [22–24]. These composite aerogels typically have a low density and porous nature and thus offer significant advantages in oil–water separation. Additives acting as a support framework can effectively prevent excessive stacking of graphene sheets, reducing the aerogel density and enhancing the original aerogel performance. However, the additive materials used in these methods are more expensive or have longer experimental cycles, which is not conducive to practical production applications. Therefore, it is crucial to control the morphology of graphene aerogels through a simple process, short experimental cycle, and low-cost method to achieve enhanced aerogel properties for practical applications.

Here, this paper creatively introduces the inexpensive industrial raw material melamine directly into the graphene aerogel framework, and melamine played the role of a supporting skeleton in the self-assembly process of graphene sheets to form the gel, preventing the three-dimensional graphene network from overstacking and forming an interconnected network with multilevel porosity. In addition, the high-temperature pyrolysis of melamine further reduced the density of the aerogel and doped the nitrogen atoms into the graphene lattice. The previous work gave a rough report on the hydrophobicity of nitrogen-doped aerogels [25], and this paper discusses in detail how melamine affects graphene at various stages and forms aerogels with excellent properties such as ultralow density (approximately 3.5 mg/cm^3), large specific surface area (133.94 m^2/g), superhydrophobic (158.2°), and excellent adsorption capacity for organic solvents (440 g/g for chloroform). More impressively, the aerogel can be selected for different recycling methods and exhibits excellent reusability in cycling. Therefore, it had great application value in dealing with marine oil spills.

Experimental

Materials

Natural flake graphite (99.95%, 325 mesh) and sodium ascorbate ($C_6H_7O_6Na$, 99%) were purchased from Aladdin. Melamine ($C_3H_6N_6$, 99.5%) was purchased from the Tianjin Institute of Fine Chemicals. Sodium ascorbate ($C_6H_7O_6Na$, 99%) was purchased from Aladdin. Hydrogen peroxide (H_2O_2, 30%) was purchased from Tianjin Zhengcheng Chemical Products Co., Ltd. Deionized water was homemade through a laboratory purified water system. All chemicals used in the experiments were of analytical grade and used as received without further purification.

Preparation of the graphene oxide suspension

According to a modified Hummers' method [26], graphene oxide (GO) was prepared from natural graphite powder. The GO suspension was prepared by centrifugation, sonication, and dispersion of GO in deionized water.

Preparation of reduced graphene oxide aerogels (NGAs)

GO prepared by Hummers' method was formulated into a 2-mg/ml graphene solution, stirred, and sonicated. Sodium ascorbate, melamine, and 30% hydrogen peroxide were sequentially added to the GO solution, where the ratios of melamine to GO were 1:0, 1:0.25, 1:0.33, 1:0.5, and 1:1. The mixed solution was stirred and sonicated until the components were homogeneous. The mixture was sealed in a certain number of ampoules and heated in an oil bath pot at 100 °C for 2 h, 4 h, 8 h, and 12 h. After the ampoules were cooled to room temperature, the ampoule was destroyed, and the obtained hydrogel was immersed in deionized water for 1 h. The washed aerogel was then freeze-dried at -80 °C for 24 h to produce melamine-modified nitrogen-doped graphene aerogel. The corresponding aerogels were denoted N_xGAs-y, where x is the mass ratio of melamine to GO, and y is the reaction time. When x equals 0, the aerogels were denoted GAs-y.

Preparation of nitrogen-doped carbon graphene aerogels (NCGAs)

Under 99.9% purity nitrogen protection, the freeze-drying aerogels were transferred to a quartz tube furnace for carbonization treatment. Heat the quartz tube furnace to 800 °C at a heating rate of 5 °C/min and hold it at 800 °C for 120 min, waiting for natural cooling to room temperature to obtain nitrogen-doped carbon graphene aerogels. The samples of NGAs after pyrolysis were designated NCGAs.

Characterization

The morphology and microstructure of the NCGAs were characterized with scanning electron microscopy (SEM, Hitachi S-4700). High-resolution X-ray photoelectron spectroscopy (XPS, ESCALAB 250) was performed to analyse the surface chemical composition and the atomic ratio of elements in CGAs-2 and NCGAs-2. An X-ray diffraction (XRD, Ultima IV) system was applied to measure the XRD patterns with Cu Kα radiation and a scanning rate of 10°/min. Raman spectra were recorded at an excitation wavelength of 633 nm using a Reflex inVia Raman microscope. The nanoscale pore size distribution and specific surface area of the NCGAs were measured via adsorption and desorption of N_2 (BET, ASAP-2460-4N) based on Brunauer–Emmett–Teller (BET) theory and the Barrett–Joyner–Halenda (BJH) method. The contact angles of CGAs and NCGAs were measured with 3-μL droplets of water using the contact angle measuring system (Dataphysics TBU 90E) at room temperature.

Density and porosity

The volume of CGAs and NCGAs was calculated by measuring the length and bottom diameter using a digital Vernier calliper, and their masses were measured using a balance with 0.1 mg accuracy. The tests were performed at room temperature and atmospheric pressure, so the density of air stored in the pores inside the aerogel was unavoidable. The density (ρ) of the graphene aerogels was calculated by Eq. (1):

$$\rho = \frac{m}{v} \tag{1}$$

Adsorption capacity and reusability

CGAs-2 or $N_{0.5}$CGAs-2 was weighed at room temperature and atmospheric pressure and then immersed in a container pre-filled with or oil organic reagents. After equilibrium of aerogel adsorption, saturated CGAs-2 or $N_{0.5}$CGAs-2 was separated from the beaker containing the organic solution and weighed. Use Eq. (2) to calculate the adsorption capacity (Q) of the aerogel.

$$Q(g/g) = (m - m_0)/m_0 \tag{2}$$

where Q is the adsorption capacity of CGAs-2 or $N_{0.5}$CGAs-2, and m_0 and m are the weights of CGAs-2 and $N_{0.5}$CGAs-2 before and after adsorption, respectively.

The adsorption capacity evaluated the reusability of $N_{0.5}$CGAs-2 after 20 adsorption–desorption cycles. Anhydrous ethanol was selected as the standard

organic solvents to test adsorption–combustion, the adsorption–desiccation of $N_{0.5}$CGAs-2 for 20 cycles, and the adsorption–combustion of $N_{0.5}$CGAs-2 for 10 cycles. Chloroform was selected as the model oil to test the adsorption–distillation of $N_{0.5}$CGAs-2 for 20 cycles.

Results and discussion

GO, as the precursor, is of great importance to the final structure and property of graphene aerogels and can be easily dispersed in pure water because of its abundant carboxyl and hydroxyl groups. The fabrication process of CGAs and $N_{0.5}$CGAs-2 is shown in Fig. 1. In the fabrication process, sodium ascorbate, melamine, and hydrogen peroxide were added to the GO suspension to synthesize the hydrogel in one step, removal of water by freeze-drying without destroying the porous structure of aerogels, and the N-doped aerogels were obtained. In order to systematically study the effect of heteroatom doping on aerogel density and to better understand the mechanism of aerogel growth, samples with different ratios of N doping were prepared. More specific details are presented in the Experimental Section. GO is reduced to rGO by sodium ascorbate and rapidly forms a porous three-dimensional network by π-π stacking. Meanwhile, melamine was physically cross-linked into the graphene network through noncovalent interactions and prevented excessive stacking of sheets. The addition of hydrogen peroxide increased the porosity of the aerogel.

Figure 2a shows a photograph of a piece of $N_{0.5}$CGAs-2 placed on cotton. Only a few outstretched cotton fibres could bear the weight of $N_{0.5}$CGAs-2, which was sufficient to show that $N_{0.5}$CGAs-2 was ultralight in mass and extremely low in density. SEM was used to characterize the surface morphology of CGAs-2 and $N_{0.5}$CGAs-2, and many pores were clearly observed in the SEM images of both CGAs-2 and $N_{0.5}$CGAs-2. The porous structure provided a large specific surface area for the aerogels and provided more adsorption sites for the aerogels, making it easier for the solvent to be transported to the surface of the aerogels, thus enhancing the adsorption capacity of the aerogels [27]. Figure 2b shows that $N_{0.5}$CGAs-2 stacked to form a more regular lamellar structure, providing a vertical channel for the entry of organic solvents. Furthermore, Fig. 2c and d shows the presence of interconnected nanosheets of $N_{0.5}$-CGAs-2, forming a honeycomb-like pore structure and open pores with a width of 20–40 μm (Fig. 2e), which facilitate the uptake of organic solvents.

In contrast, CGAs-2 exhibited a more disordered microstructure, as shown in Fig. 2f, g, and a smaller number of pores relative to $N_{0.5}$CGAs-2. The presence of lamellar and honeycomb structures and open pores of $N_{0.5}$CGAs-2 enhanced the capillary flow of oil and organic solvents [28]. The main reason for the excellent dispersion of graphene lamellae in the $N_{0.5}$CGAs-2 network was that melamine effectively prevented severe aggregation and restacking between graphene lamellae during the gel generation process, increasing the specific surface area. In addition, the specific surface area of $N_{0.5}$CGAs-2 (Fig. S1a, 133.94 m^2/g) is much larger than the specific surface area of CGAs-2 (Fig. S1b, 67.68 m^2/g). The layered channel and honeycomb structure enable $N_{0.5}$CGAs-2 to compress and restore its original shape quickly after removing the external force. First, in gelation, the cross-linking effect of melamine made the graphene sheets stack effectively to form a more regular and ordered structure. Second, after pyrolyzing melamine at high temperature, new voids

Figure 1 Scheme of the synthetic procedure for the preparation of the rGO/melamine porous aerogel.

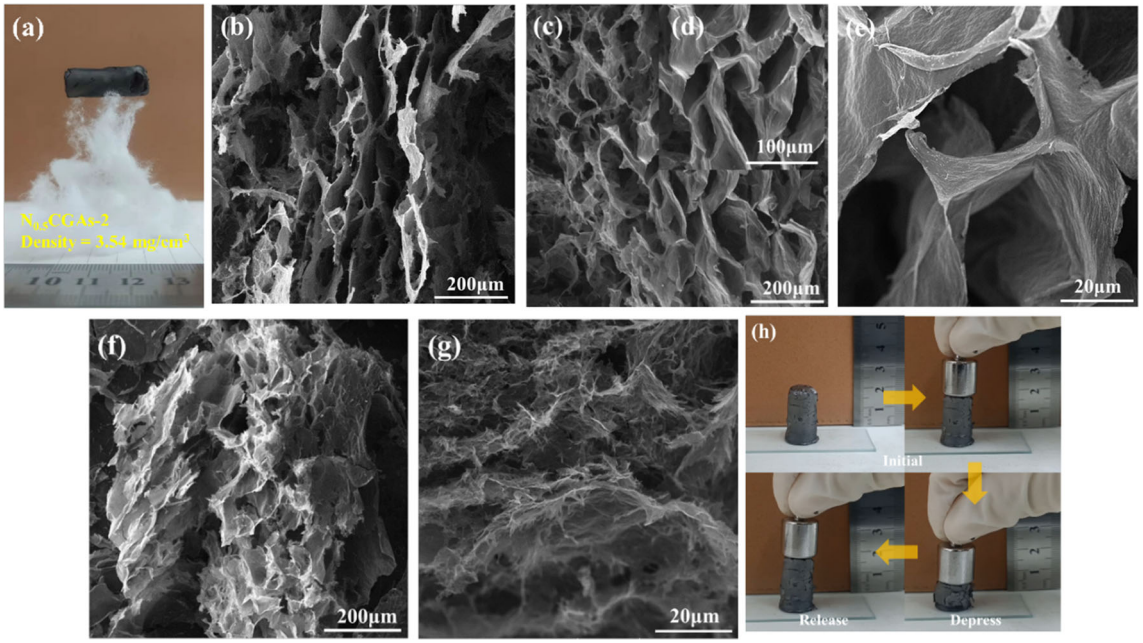

Figure 2 Structural characterization of aerogels. **a** Photograph of $N_{0.5}$CGAs-2 placed on the cotton. **B**, **c**, **d** and **e** SEM photos of $N_{0.5}$CGAs-2 at different scales. **f** and **g** SEM photos of CGAs-2 at different scales. **h** Snapshots demonstrate the super compressibility of the $N_{0.5}$CGAs-2.

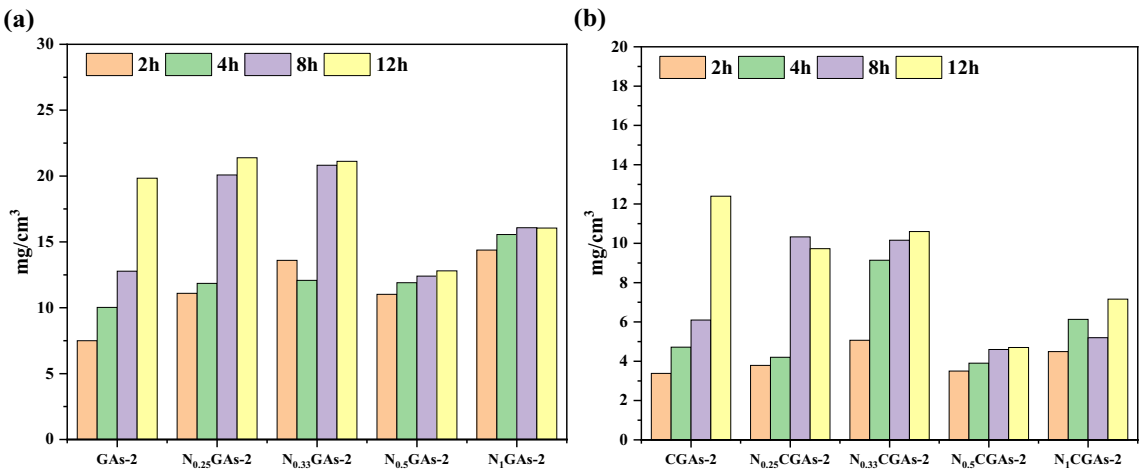

Figure 3 **a** Density changes of GAs and NGAs under different doping ratios and times. **b** Density changes of CGAs and NCGAs under different doping ratios and times.

were formed in the original position, leading to $N_{0.5}$CGAs-2 having an elastic frame. As shown in Fig. 2h, during the extrusion of $N_{0.5}$CGAs-2, the height of $N_{0.5}$CGAs-2 was compressed by nearly 50%. After removing the external force, $N_{0.5}$CGAs-2 fully recovered to its original height and shape, and no obvious macroscopic deformation was observed.

The volume changes before and after carbonization were almost negligible, indicating that the presence of graphene provided a carbon skeleton with good dimensional stability for the aerogel, and melamine would not destroy the stable three-dimensional structure of the aerogel during the pyrolysis process. Melamine played a role in supporting the skeleton during the graphene stacking process, effectively preventing excessive stacking of the lamellae and enabling the formation of a network with high-porosity interconnections.

Figure 3a and b shows the change in aerogel density with different doping ratios and different reaction times and further analyses the role of melamine in the system. GA-2 had a density of 7.5 mg/cm^3, CGA-2 had a density of 3.38 mg/cm^3, GA-12 had a density of 19.84 mg/cm^3, and GA-12 had a density of 12.4 mg/cm^3. The density changes of GAs and CGAs were much more significant than those of NGAs and NCGAs with increasing the time spent stacking graphene into a gel. We believe that as the gelation time increases, the aerogel stacks become tighter, and the gap between the lamellae becomes smaller. Melamine acts as a cross-linking agent, effectively preventing any further reduction in the gap between graphene sheets and forming an ordered stacking structure. In addition, Fig. 3b shows that the NCGAs lost significantly more weight than the CGAs during carbonization due to the decomposition of melamine during carbonization, which further reduced the density of the aerogels while doping nitrogen atoms into the graphene lamellae. The apparent density of $N_{0.5}$CGAs and N_1CGAs did not change much in the reaction time range of 2–12 h, indicating that the graphene sheet stacking process was relatively perfect after 2 h, and it was difficult to further reduce the interlayer gap with increasing reaction time. Compared with that of $N_{0.5}$CGAs, the overall density of N_1CGAs increased, which should be due to the incomplete decomposition of melamine during the carbonization process, resulting in improved aerogel quality. Among the different doping ratios, $N_{0.5}$CGAs had less apparent density variation in the reaction time range of 2–12 h and the lightest average density of approximately 4 mg/cm^3, making its more theoretically applicable.

Chemical properties and water contact angle

The elemental compositions and nitrogen bond configurations in CGAs-2 and NCGAs-2 were analysed by x-ray photoelectron spectroscopy (XPS). As shown in Fig. 4a, the XPS spectrum of CGAs-2 only indicated the presence of carbon and oxygen atoms, while the XPS spectrum of the NCGAs-2 sample clearly showed the intercalation of nitrogen atoms into the graphene network. XPS elemental analysis (Table 1) showed the atomic proportions of CGAs-2 and NCGAs-2. The nitrogen content of NCGAs-2 increased with the proportion of melamine in the system. Therefore, the ratio of graphene and melamine in the system could be controlled during the gelation stage, thereby realizing NCGAs-2 with

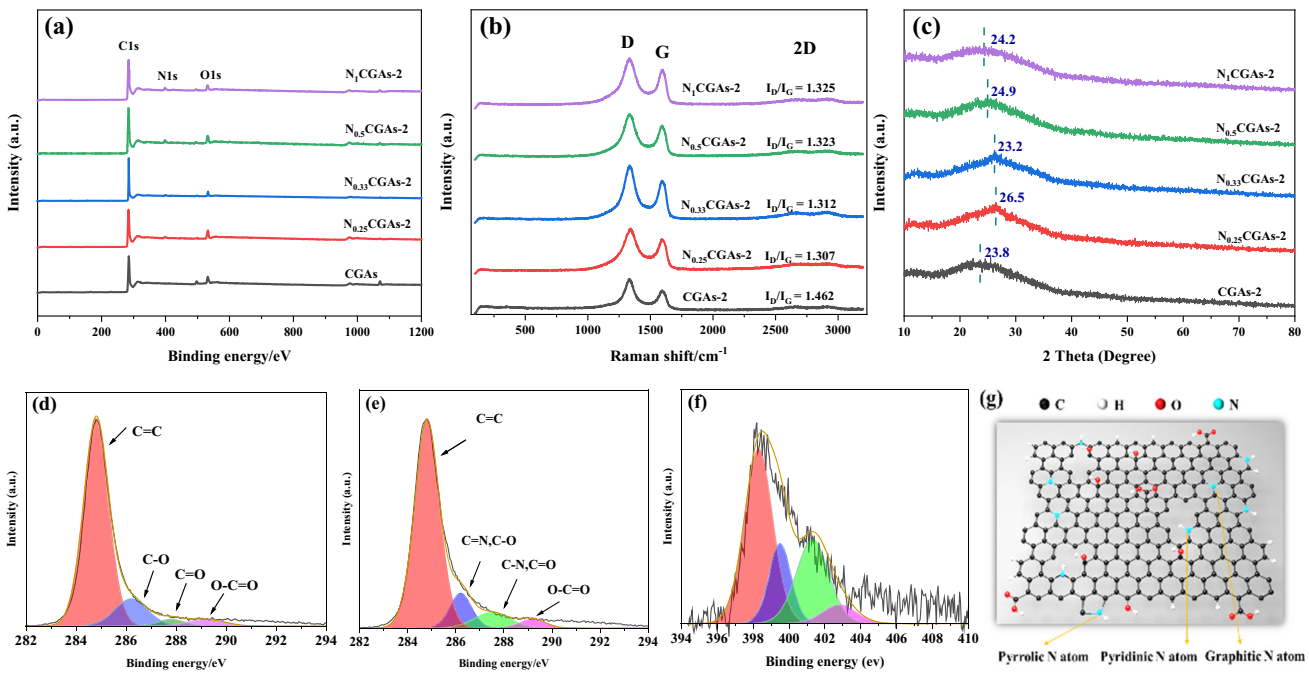

Figure 4 **a** General XPS spectra of CGAs-2 and $N_{0.5}$CGAs-2. **b** Raman spectra of CGAs-2 and $N_{0.5}$CGAs-2. **c** XRD spectra of CGAs-2 and $N_{0.5}$CGAs-2. High-resolution C1s XPS spectra of **d** CGAs-2 and **e** $N_{0.5}$CGAs-2. (f) High-resolution N1s XPS spectra of $N_{0.5}$CGAs-2. **g** Schematic structure of NCGAs.

Table 1 Detailed XPS data of CGAs-2 and NCGAs-2

Sample	C (at%)	O (at%)	N (at%)
CGAs-2	90.94	9.06	0
$N_{0.25}$CGAs-2	88.84	8.81	2.35
$N_{0.33}$CGAs-2	90.96	5.84	3.2
$N_{0.5}$CGAs-2	89.87	6.6	3.53
N_1CGAs-2	90.49	5.17	4.34

different nitrogen doping ratios. In addition, the O content continued to decrease as the N content increased, which indicated that the removal of oxygen-containing groups on the graphene surface provided active sites for nitrogen doping into the graphene lattice. In the graphene lattice, carbon atoms that connect to oxygen-containing groups were more easily replaced by nitrides generated by the pyrolysis of melamine at high temperatures, which is consistent with the conclusions obtained by the previous researchers [29].

The structures of CGAs-2 and NCGAs-2 were further analysed using Raman spectroscopy (Raman) and X-ray diffraction (XRD). Figure 4b shows the Raman spectra of CGAs-2 and NCGAs-2, with two remarkable bands at approximately 1337 cm^{-1} and 1593 cm^{-1}, which can be assigned to the D- and G-bands of carbon, respectively. Specifically, the D peak was generally considered the disordered vibrational peak of graphene, which was caused by lattice vibrations far from the Brillouin centre and was used to characterize structural defects or disordered structures in graphene. The G peak was the prominent characteristic peak of graphene caused by the in-plane vibration of carbon atoms and was used to characterize the degree of graphitization of graphene. The intensity ratio (I_D/I_G) of the D- and G-bands is usually used to measure the defect level of graphite materials [22, 30]. The addition of H_2O_2 in the preparation process to generate more holes increased the number of defects and disordered structures of CGAs-2, which resulted in an I_D/I_G ratio of CGAs-2 of 1.462. The I_D/I_G of NCGAs-2 was lower than that of CGAs-2, indicating that the regularity of NCGAs-2 was higher than that of CGAs-2, which indicated that the nitride introduced by melamine cleavage could repair the lattice structure of graphene to some extent. However, with the increase in nitrogen content, the I_D/I_G ratio of NCGAs-2 gradually increased. The degree of disorder of NCGAs slightly increased with the doping ratio, which was caused by the augmentation of the disorder degree caused by the incomplete decomposition of more melamine at high temperatures with the increase in doping ratio.

X-ray diffraction (XRD) is an effective method used to study the microstructure of crystalline substances and certain amorphous substances. Figure 4c shows the XRD patterns of CGAs-2 and NCGAs-2. CGAs-2 showed a broad peak at $2\theta = 23.8°$ (d-spacing = 0.38 nm), corresponding to the diffraction of the graphitic carbon (002) plane, which means that reduced graphene oxide formed [31]. Relative to that of CGAs-2, the peak position of NCGAs-2 shifted to the right, and the broad peak of $N_{0.25}$CGAs-2 appeared at 26.5° (d-spacing = 0.34 nm). However, with increasing nitrogen content, the broad peak of NCGAs-2 gradually shifted, and the broad peak positions of N_1CGAs-2 ($2\theta = 24.2°$, d-spacing = 0.38 nm) and CGAs-2 almost coincided. The reduction in interlayer space reflected the elimination of oxygen-containing functional groups to a certain extent [5], which also indicated that high-temperature melamine cleavage products had specific reducing properties, which could reduce the oxygen content of graphene and shorten the gap between graphene sheets. However, melamine played a supportive role in the gelation stage by preventing excessive stacking of graphene lamellae and increasing the layer spacing. As the proportion of melamine in the system increased, the spacing between graphene sheets in NCGAs-2 gradually expanded. The XPS, Raman, and XRD results of CGAs-2 and NCGAs-2 indicate that the nitrides produced by melamine had a reducing effect, which attacked the oxygen-containing group active sites at high temperature and partially restored the graphite lattice structure.

The high-resolution C1s XPS spectra (Fig. 4d and e) of CGAs-2 and NCGAs-2 showed one main peak at 284.4–285.0 eV, corresponding to sp2-hybridized graphitic carbon atoms and small signals at higher binding energies, indicating that some C-N or C-O species remained in CGAs-2 and NCGAs-2 [32]. In the C1s spectra of CGAs-2 and NCGAs-2, the sharp peak at 284.8 eV corresponding to sp2 carbon atoms indicated that most of the carbon atoms were in the form of a conjugated honeycomb lattice. The 286.2 eV, 287.8 eV, and 289.2 eV peaks correspond to oxygen-containing groups such as C-O/C = N, C = O/C-N, and O-C = O, respectively [29]. Similarly, the high-resolution N1s spectra (Fig. 4f) of

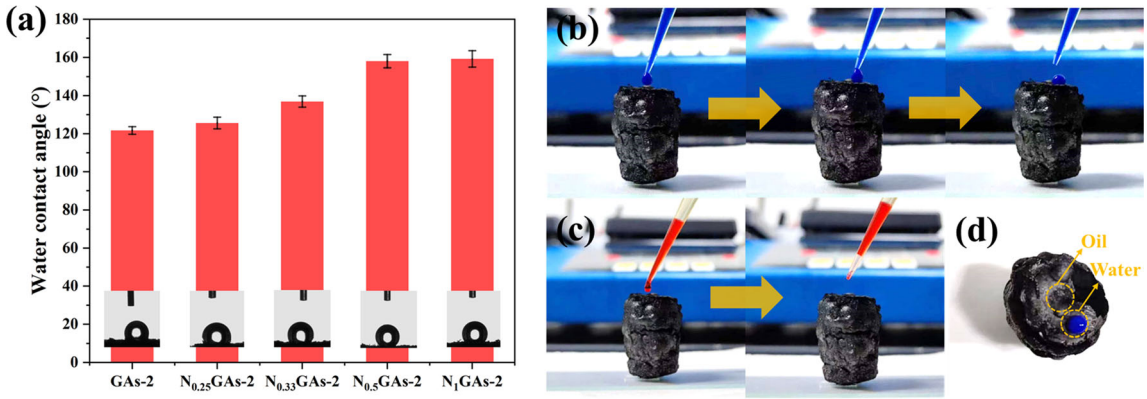

Figure 5 **a** Water contact angle of CGAs-2 and CGAs-2. **b** Water droplets (dyed blue by blue ink) remain on the $N_{0.5}$CGAs-2 surface. **c** Oil droplets (dyed red by Sudan III) are quickly adsorbed on the $N_{0.5}$CGAs-2 surface. **d** $N_{0.5}$CGAs-2 surface after adding water and oil droplets.

$N_{0.5}$CGAs-2 could be fitted to four peaks at 398.2, 399.5, 401.1, and 402.6 eV, corresponding to pyridinic-N, pyrrolic-N, graphitic-N, and oxidized nitrogen peak (as illustrated in Fig. 4g), respectively [24, 29, 33]. In the previous work, Sheng et al. suggested that pyridinic-N determines the electrocatalytic ORR activity of nitrogen-doped graphene [29]. $N_{0.5}$CGAs-2 exhibits a high nitrogen doping content and thus has potential applications for electrocatalysis in the ORR.

As depicted in Fig. 5(a), the water contact angle gradually increased with the increase in melamine content in the system. The water contact angle of CGAs-2 was 122.5° while that of $N_{0.5}$CGAs-2 was 158.2°, which corresponds to the previous characterization results. The pyrolysis of melamine under high-temperature conditions replaces the oxygen atoms on the graphene oxide surface, leading to a reduction in hydrophilic groups on the graphene lamellae. As a result, the water contact angle of the aerogel increases on a macroscopic scale. The abrupt change from $N_{0.33}$CGAs-2 to N0.5CGAs-2 in the water contact angle may be attributed to the formation of a more regular lamellae structure, which enhances the hydrophobicity of the aerogel by increasing its roughness and forming an air barrier between water droplets and the aerogel surface (as described in [34, 35]). The sequence of events is clearly illustrated in Fig. 5b, where water droplets fall on the $N_{0.5}$CGAs-2 aerogel but cannot be adsorbed, whereas oil droplets are instantaneously adsorbed by $N_{0.5}$CGAs-2 (Fig. 5c). Figure 5d shows the aerogel surface after the test. The superhydrophobic properties make $N_{0.5}$CGAs-2 a promising candidate for marine oil spill treatment and provide a theoretical basis for the oil–water selectivity described below.

Adsorption properties and reusability

Due to its porous structure, large surface area, low density, and excellent mechanical stability, the $N_{0.5}$-CGAs-2 aerogel should be a promising adsorber for oil and other organic pollutants. The adsorption selectivity of the aerogels was analysed by contacting $N_{0.5}$-CGAs-2 with underwater chloroform (dyed red by Sudan III). The rapid adsorption of dyed chloroform was observed within one second, and the adsorption of chloroform was complete in three seconds (Movie S1). The adsorption of oil slicks on water was then tested, and hexane was also adsorbed within seconds (Movie S2). In this process, the aerogel adsorbs organic solvents selectively and leaves behind pure water (Fig. 6).

Due to its ultra-lightweight, low density, oil–water selectivity, and compressibility recoverability, $N_{0.5}$-CGAs-2 has significant advantages in removing pollutants such as oil and organic solvents and is an ideal candidate as an adsorbent, which was fully confirmed by various solvent adsorption experiments. Therefore, we have tested the adsorption capacity of $N_{0.5}$CGAs-2 and CGAs-2 using various oils or organic reagents. These oils or organic solvents are common organic pollutants in daily life and industrial production and include chloroform, tetrachloromethane, peanut oil, hexane, silicone oil, N–N-dimethylformamide, ethanol, glycol, tetraethyl orthosilicate, ethylenediamine, and tetrahydrofuran.

In tests on different oils and solvents, $N_{0.5}$CGAs-2 exhibits excellent adsorption capacity ranging from 188 to 440 time, even peanut oil with high viscosity

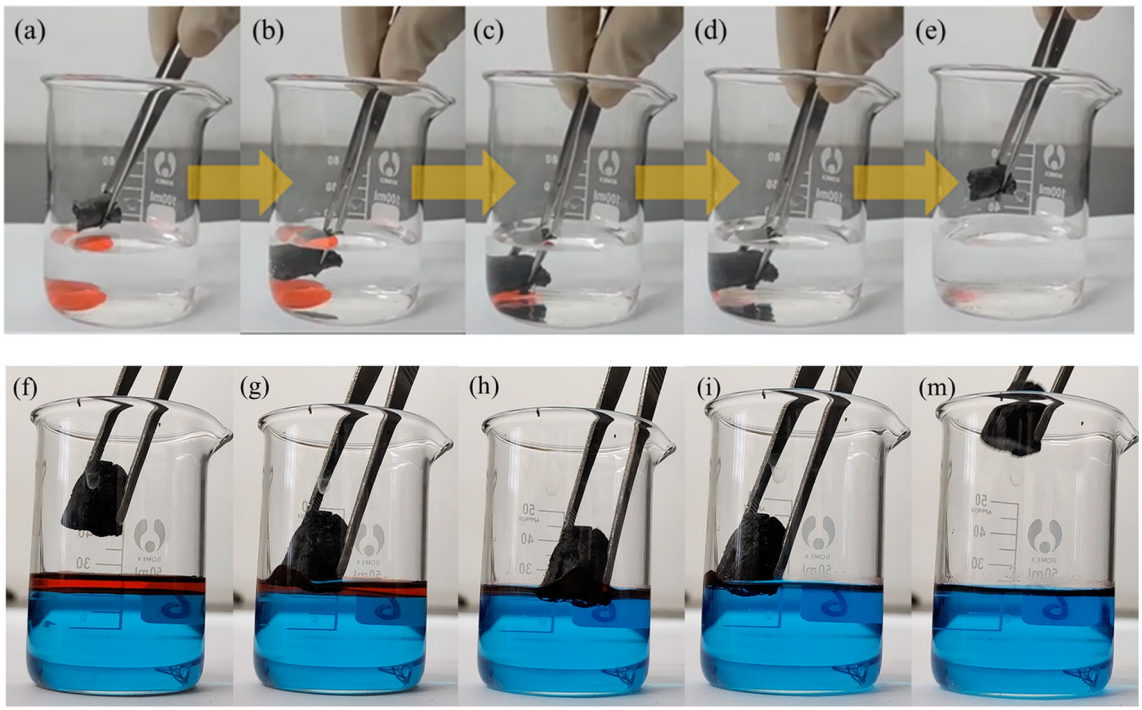

Figure 6 **a**–**e** Selectively remove chloroform (dyed red by Sudan III) from the water using $N_{0.5}$CGAs-2. **f**–**m** Removal of light oil (n-Hexane, dyed red by Sudan III) from the water (dyed blue by blue ink) surface using $N_{0.5}$CGAs-2.

(Fig. 7a). As Fig. 7b shows, the adsorption capacity of $N_{0.5}$CGAs-2 was significantly higher than that of CGAs-2 (adsorption capacity ranging from 141 to 342 times). Aerogels adsorption of oil or organic solvents is mainly a physical process rather than a chemical combination, and the density and viscosity of the adsorbent solvent directly affect the magnitude of the adsorption capacity [36]. The adsorption capacities of $N_{0.5}$CGAs-2 and CGAs-2 were consistent with the microscopic characterization results of aerogels. The capillary effect was considered to be the driving force for the adsorption and transfer of oil and organic solvents into the aerogel, and the oil and organic solutions entering the aerogel could spontaneously enter the aerogel through capillary action [37, 38]. The rich laminar porous structure, honeycomb-like structure, and larger specific surface area of $N_{0.5}$-CGAs-2 provided more adsorption sites, richer capillary channels, and broader oil storage space for the adsorption of oil and organic solvents. Therefore, the adsorption capacity of $N_{0.5}$CGAs-2 is higher than that of CGAs-2.

More importantly, compared with the oil-adsorbing capacity of the reported oil-adsorbing materials, as listed in Table 2, the oil-adsorbing capacity of $N_{0.5}$CGAs-2 showed a clear advantage. Due to the simple synthesis method, short cycle time, and low drug cost, the prepared $N_{0.5}$CGAs-2 has broad and essential application prospects for oil cleanup and industrial wastewater treatment. Most pollutants are toxic or valuable raw materials, and porous adsorbent materials [48] can be recycled post-treatment after the adsorption of pollutants to achieve energy cost savings. Therefore, recyclability and reusability are critical indicators for assessing the application of adsorbent materials. Different methods can be used for different types of contaminants. Toxic or nonrecoverable organic contaminants can be removed by drying or combustion, and expensive reagents can be recovered by distillation [46, 49]. To demonstrate the cyclic uptake ability of $N_{0.5}$CGAs-2, we first performed adsorption–drying–adsorption, adsorption–combustion–adsorption, and adsorption–squeezing–adsorption experiments using ethanol as a model oil. After $N_{0.5}$CGAs-2 adsorbed ethanol, it was dried directly in a drying oven at 60 °C for one hour. The cycle was repeated 20 times, and the minimum adsorption amount was 89.2% of the first adsorption amount (Fig. 8a), which indicated that the $N_{0.5}$CGAs-2 aerogel had excellent thermal stability. The saturated adsorbed $N_{0.5}$CGAs-2 was ignited, and the adsorbed solvent was removed directly by

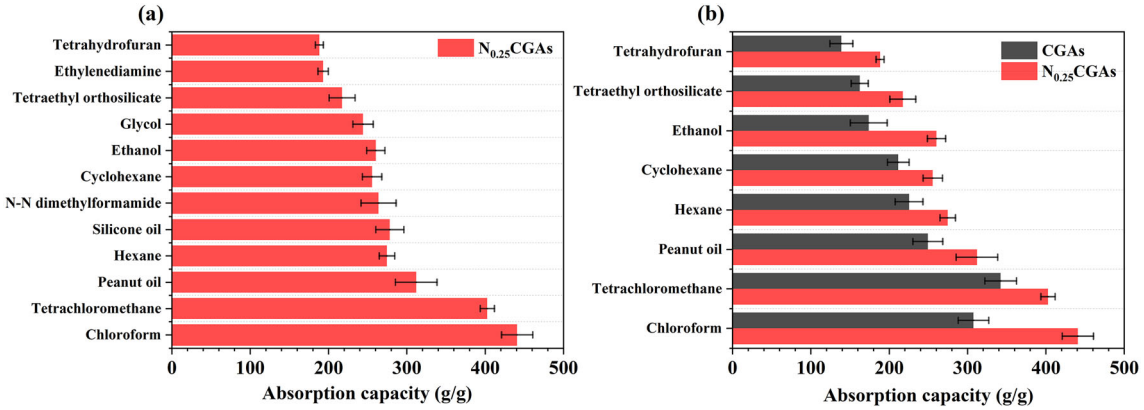

Figure 7 **a** The adsorption capacity of $N_{0.5}$CGAs-2 toward different kinds of oil and organic solvents. **b** The adsorption capacity of CGAs-2 and $N_{0.5}$CGAs-2 for various oils and solvents.

Table 2 Comparison of various graphene aerogels

Adsorbent material	Maximum adsorption capacity (g/g)	Lowest density (mg/cm^3)	Refs
Graphene/ethylenediamine aerogel	250	4.4	[39]
Graphene/cysteamine aerogel	310	4.2	[11]
Graphene/cellulose aerogel	197	5.9	[40]
Spongy Graphene	86	12	[41]
Anisotropic graphene aerogels	200	4	[42]
Graphene/polyvinyl alcohol/cellulose nanofiber aerogel	287	6.17	[43]
Carbon aerogels derived from sisal fibers	188		[44]
Graphene/nanofibrillated cellulose aerogel	265	5.6	[45]
Carbon nanotubes/graphene hybrid aerogel	83	6.2	[46]
Graphene Aerogel Millispheres	195	5.0	[47]
This work	440	3.5	

combustion (Fig. 8b, Movie S3). After 10 combustion cycles, the adsorption decreased to 70.2% of the initial capacity. Due to its high initial adsorption capacity, even if the final adsorption efficiency dropped to 50.6%, its adsorption capacity was still as high as 105 g/g. Subsequently, to further test the refractoriness, $N_{0.5}$CGAs-2 without adsorbed organic solvents was placed on the flame of the alcohol lamp for 1 min (Fig. 9, Movie S4). Its macrostructure showed slight carbonization marks on the surface, and overall structure is not damaged. And under the same conditions, the fire resistance of CGAs-2 is significantly inferior to that of $N_{0.5}$CGAs-2 (Fig. S2, Movie S5). These results show that the $N_{0.5}$CGAs-2 aerogel had good fire resistance and excellent structural stability, the adsorbed organic solvent could be easily removed using drying and in situ combustion, and the aerogel still maintained its basic framework without collapsing or burning in the air. The direct extrusion method was more attractive than easy heat treatment because it was highly effective in terms of energy consumption and ease of operation. The pressure was applied in the axial direction, with $N_{0.5}$CGAs-2 adsorbed with saturated ethanol, for approximately 50% deformation. After 10 cycles of the adsorption–extrusion operation, the minimum adsorption amount was 89% of the first adsorption amount, which indicates that $N_{0.5}$CGAs-2 has good flexibility and structural stability (Fig. 8c). Distillation was suitable for removing expensive contaminants or those with low boiling points. Distillation was more economical and environmentally friendly than direct drying or combustion; distillation did not require secondary treatment, unlike direct extrusion. We performed adsorption–distillation–adsorption experiments using chloroform as the model oil. Distillation was performed for one hour at a temperature slightly above the boiling point and repeated 20 times, and the minimum adsorption amount was approximately 83% of the first adsorption amount (Fig. 8d).

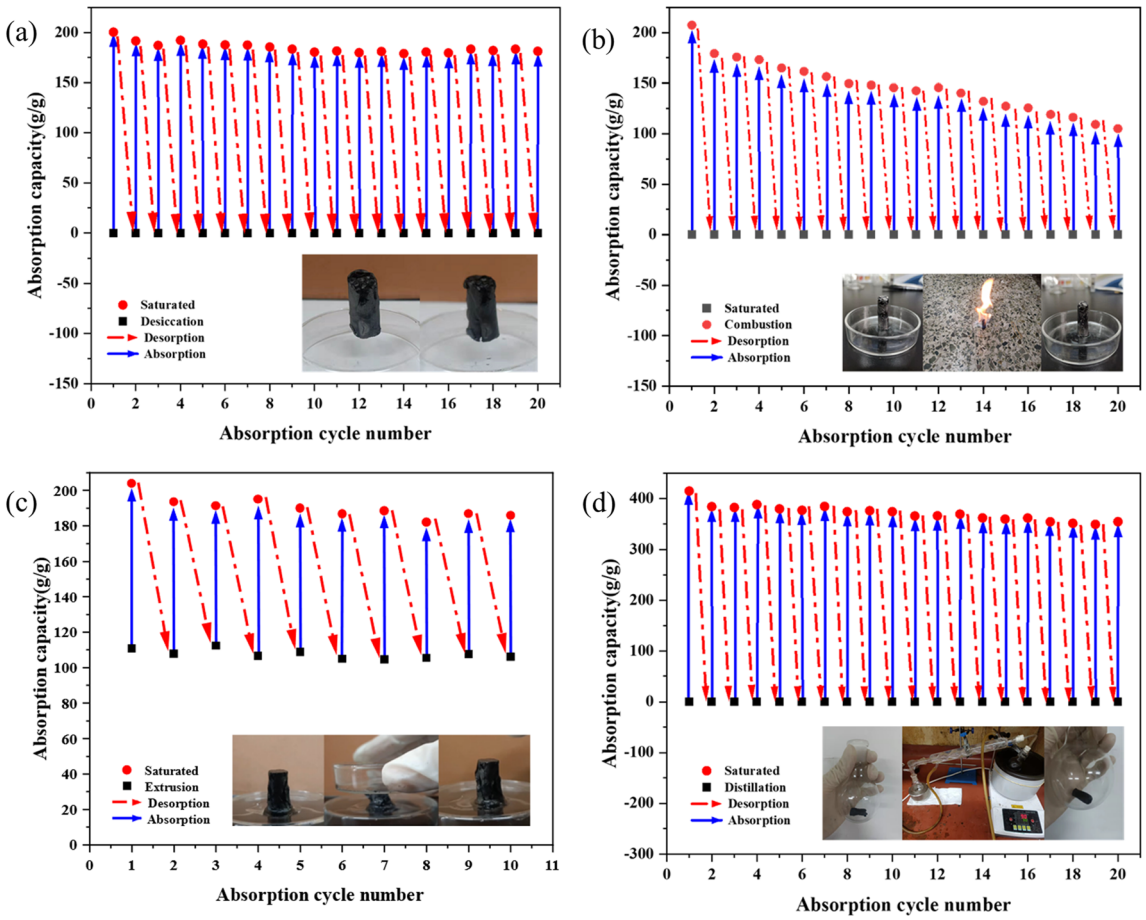

Figure 8 **a** Ethanol adsorption-desiccation and recoverability testing of $N_{0.5}$CGAs-2. **b** Ethanol adsorption-combustion and recoverability testing of $N_{0.5}$CGAs-2. **c** Ethanol adsorption-extrusion and recoverability testing of $N_{0.5}$CGAs-2. **d** Chloroform adsorption- Distillation and recoverability testing of $N_{0.5}$CGAs-2.

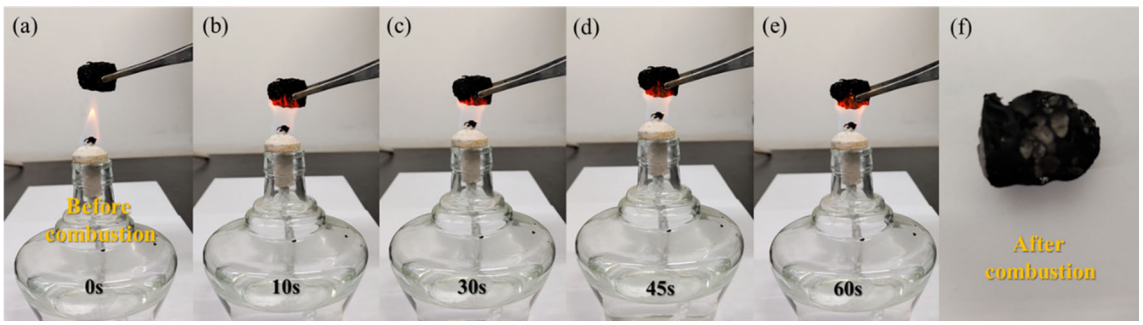

Figure 9 Process of $N_{0.5}$CGAs-2 under the combustion of alcohol lamp lasting for different time.

Conclusions

In summary, this study utilizes the inexpensive industrial raw material melamine in combination with graphene to prepare ultralight, structurally stable, and repressively compressible aerogels with applications for the efficient adsorption of oil and organic solvent pollutants. Compared with most of the current ultralight materials, the preparation method is simple and inexpensive and is expected to be applied in industrial production. Melamine cross-links three-dimensional graphene networks during gel formation and prevents excessive stacking of lamellae. High-temperature pyrolysis of melamine

further reduces the aerogel density and expands the pore size. The capillary channels and honeycomb-like pore structure formed by the stacked $N_{0.5}$CGAs-2 lamellae facilitate the uptake and transfer of oil and organic solvents, providing the basis for their ultra-high adsorption capacity. $N_{0.5}$CGAs-2 has an adsorption capacity of up to 440 times its mass for organic contamination, higher than that of most reported adsorption materials. The recovery method of $N_{0.5}$CGAs-2 can be selected according to the type of contaminant, maintaining nearly 90% adsorption capacity after 20 adsorption–desorption cycles. The prepared $N_{0.5}$CGAs-2 has the advantages of ultralow density, high adsorption capacity, excellent recovery capacity, good selectivity, low cost, simple process flow, environmental protection, etc. It is ideal for oil spill cleanup and has a high application value in addressing the increasing oil spill accidents and severe water pollution caused by chemical spills.

Author Contributions

RZ: Methodology, experimentation, Validation, Formal analysis, Investigation, Writing—Original draft, Software, Visualization, Resources. LL: Formal analysis, Investigation, Writing-Review & Editing, Project administration. QM: Conceptualization, Directions, Writing-Review & Editing, Supervision, Project administration, funding acquisition.

Data and code availability

The data that support the findings of this study are freely available on request from the corresponding author.

Declarations

Conflict of interest The authors declare no conflict of interest.

References

[1] Beyer J, Trannum HC, Bakke T, Hodson PV, Collier TK (2016) Environmental effects of the deepwater horizon oil spill: a review. Mar Pollut Bull 110:28–51. https://doi.org/10.1016/j.marpolbul.2016.06.027

[2] Gong J, Chen X, Tang T (2019) Recent progress in controlled carbonization of (waste) polymers. Prog Polym Sci 94:1–32. https://doi.org/10.1016/j.progpolymsci.2019.04.001

[3] Ge J, Zhao H-Y, Zhu H-W, Huang J, Shi L-A, Yu S-H (2016) Advanced sorbents for oil-spill cleanup: recent advances and future perspectives. Adv Mater 28:10459–10490. https://doi.org/10.1002/adma.201601812

[4] Bonisoli-Alquati A, Stouffer PC, Turner RE, Woltmann S, Taylor SS (2016) Incorporation of deepwater horizon oil in a terrestrial bird. Environ. Res. Lett. 11:114023. https://doi.org/10.1088/1748-9326/11/11/114023

[5] Zhan W, Yu S, Gao L, Wang F, Fu X, Sui G, Yang X (2018) Bioinspired assembly of carbon nanotube into graphene aerogel with "cabbagelike" hierarchical porous structure for highly efficient organic pollutants cleanup. ACS Appl Mater Interfaces 10:1093–1103. https://doi.org/10.1021/acsami.7b15322

[6] Yuan H, Hao R, Sun H, Zeng W, Lin J, Lu S, Yu M, Lin S, Li J, Chen L (2022) Engineered Janus cellulose membrane with the asymmetric-pore structure for the superhigh-water flux desalination. Carbohyd Polym 291:119601. https://doi.org/10.1016/j.carbpol.2022.119601

[7] Yan W, Liu L, Dong C, Xie S, Zhao X, Gao C (2021) Surface modification of reverse osmosis membrane with tannic acid for improving chlorine resistance. Desalination. 498:114639. https://doi.org/10.1016/j.desal.2020.114639

[8] Lin J, Shang Y, Ding B, Yang J, Yu J, Al-Deyab SS (2012) Nanoporous polystyrene fibers for oil spill cleanup. Mar Pollut Bull 64:347–352. https://doi.org/10.1016/j.marpolbul.2011.11.002

[9] Cheng H, Gu B, Pennefather MP, Nguyen TX, Phan-Thien N, Duong HM (2017) Cotton aerogels and cotton-cellulose aerogels from environmental waste for oil spillage cleanup. Mater Des 130:452–458. https://doi.org/10.1016/j.matdes.2017.05.082

[10] Bi H, Yin Z, Cao X, Xie X, Tan C, Huang X, Chen B, Chen F, Yang Q, Bu X, Lu X, Sun L, Zhang H (2013) Carbon fiber aerogel made from raw cotton: a novel, efficient and recyclable sorbent for oils and organic solvents. Adv Mater 25:5916–5921. https://doi.org/10.1002/adma.201302435

[11] Dai C, Sun W, Xu Z, Liu J, Chen J, Zhu Z, Li L, Zeng H (2020) Assembly of ultralight dual network graphene aerogel with applications for selective oil adsorption. Langmuir 36:13698–13707. https://doi.org/10.1021/acs.langmuir.0c02664

[12] Ren R-P, Li W, Lv Y-K (2017) A robust, superhydrophobic graphene aerogel as a recyclable sorbent for oils and organic solvents at various temperatures. J Colloid Interface Sci 500:63–68. https://doi.org/10.1016/j.jcis.2017.01.071

[13] Gao X, Wang X, Ouyang X, Wen C (2016) Flexible superhydrophobic and superoleophilic MoS_2 sponge for highly efficient oil-water separation. Sci Rep 6:27207. https://doi.org/10.1038/srep27207

[14] Chu Z, Feng Y, Seeger S (2015) Oil/water separation with selective superantiwetting/superwetting surface materials. Angew Chem Int Ed 54:2328–2338. https://doi.org/10.1002/anie.201405785

[15] Li C, Yang J, Pachfule P, Li S, Ye M-Y, Schmidt J, Thomas A (2020) Ultralight covalent organic framework/graphene aerogels with hierarchical porosity. Nat Commun 11:4712. https://doi.org/10.1038/s41467-020-18427-3

[16] Xu Y, Sheng K, Li C, Shi G (2010) Self-assembled graphene hydrogel *via* a one-step hydrothermal process. ACS Nano 4:4324–4330. https://doi.org/10.1021/nn101187z

[17] Jiang Y, Shao H, Li C, Xu T, Zhao Y, Shi G, Jiang L, Qu L (2016) Versatile graphene oxide putty-like material. Adv Mater 28:10287–10292. https://doi.org/10.1002/adma.201603284

[18] Kabiri S, Tran DNH, Altalhi T, Losic D (2014) Outstanding adsorption performance of graphene–carbon nanotube aerogels for continuous oil removal. Carbon 80:523–533. https://doi.org/10.1016/j.carbon.2014.08.092

[19] Zhao Y, Hu C, Hu Y, Cheng H, Shi G, Qu L, Versatile A (2012) Ultralight, nitrogen-doped graphene framework. Angew Chem Int Ed 51:11371–11375. https://doi.org/10.1002/anie.201206554

[20] Wang W, Jin J, Wu Y, Zhang W, Jiang H, Li X, Wang G (2019) Unique holey graphene/carbon dots frameworks by microwave-initiated chain reduction for high-performance compressible supercapacitors and reusable oil/water separation. J Mater Chem A 7:22054–22062. https://doi.org/10.1039/C9TA06083A

[21] Li L, Li B, Zhang J (2016) Dopamine-mediated fabrication of ultralight graphene aerogels with low volume shrinkage. J Mater Chem A 4:512–518. https://doi.org/10.1039/C5TA08829A

[22] Du D, Li P, Ouyang J (2015) Nitrogen-doped reduced graphene oxide prepared by simultaneous thermal reduction and nitrogen doping of graphene oxide in air and its application as an electrocatalyst. ACS Appl Mater Interfaces 7:26952–26958. https://doi.org/10.1021/acsami.5b07757

[23] Akada K, Terasawa T, Imamura G, Obata S, Saiki K (2014) Control of work function of graphene by plasma assisted nitrogen doping. Appl. Phys. Lett. 104:131602. https://doi.org/10.1063/1.4870424

[24] Zhang C, Fu L, Liu N, Liu M, Wang Y, Liu Z (2011) Synthesis of nitrogen-doped graphene using embedded carbon and nitrogen sources. Adv Mater 23:1020–1024. https://doi.org/10.1002/adma.201004110

[25] Zhang R, Meng Q (2023) Ultralight, superhydrophobic, low-cost nitrogen-doped graphene aerogels with "honeycomb" porous structure for efficient oil removal. New J Chem. https://doi.org/10.1039/D2NJ05828F

[26] Marcano DC, Kosynkin DV, Berlin JM, Sinitskii A, Sun Z, Slesarev A, Alemany LB, Lu W, Tour JM (2010) Improved synthesis of graphene oxide. ACS Nano 4:4806–4814. https://doi.org/10.1021/nn1006368

[27] Feng J, Nguyen ST, Fan Z, Duong HM (2015) Advanced fabrication and oil adsorption properties of super-hydrophobic recycled cellulose aerogels. Chem Eng J 270:168–175. https://doi.org/10.1016/j.cej.2015.02.034

[28] Song Z, Duan H, Zhu D, Lv Y, Xiong W, Cao T, Li L, Liu M, Gan L (2019) Ternary-doped carbon electrodes for advanced aqueous solid-state supercapacitors based on a "water-in-salt" gel electrolyte. J Mater Chem A 7:15801–15811. https://doi.org/10.1039/C9TA02690H

[29] Sheng Z-H, Shao L, Chen J-J, Bao W-J, Wang F-B, Xia X-H (2011) Catalyst-free synthesis of nitrogen-doped graphene *via* thermal annealing graphite oxide with melamine and its excellent electrocatalysis. ACS Nano 5:4350–4358. https://doi.org/10.1021/nn103584t

[30] Yeom D-Y, Jeon W, Tu NDK, Yeo SY, Lee S-S, Sung BJ, Chang H, Lim JA, Kim H (2015) High-concentration boron doping of graphene nanoplatelets by simple thermal annealing and their supercapacitive properties. Sci Rep 5:9817. https://doi.org/10.1038/srep09817

[31] Ma G, Guo D, Sun K, Peng H, Yang Q, Zhou X, Zhao X, Lei Z (2015) Cotton-based porous activated carbon with a large specific surface area as an electrode material for high-performance supercapacitors. RSC Adv 5:64704–64710. https://doi.org/10.1039/C5RA11179J

[32] Jeong H-K, Lee YP, Lahaye RJWE, Park M-H, An KH, Kim IJ, Yang C-W, Park CY, Ruoff RS, Lee YH (2008) Evidence of graphitic AB stacking order of graphite oxides. J Am Chem Soc 130:1362–1366. https://doi.org/10.1021/ja076473o

[33] Xu F, Minniti M, Barone P, Sindona A, Bonanno A, Oliva A (2008) Nitrogen doping of single walled carbon nanotubes by low energy N^{2+} ion implantation. Carbon 46:1489–1496. https://doi.org/10.1016/j.carbon.2008.06.047

[34] Liu L, Shan X, Hu X, Lv W, Wang J (2021) Superhydrophobic silica aerogels and their layer-by-layer structure for thermal management in harsh cold and hot environments. ACS Nano 15:19771–19782. https://doi.org/10.1021/acsnano.1c07184

[35] Zhang X, Lei Y, Li C, Sun G, You B (2022) Superhydrophobic and multifunctional aerogel enabled by bioinspired salvinia leaf-like structure. Adv Funct Materials 32:2110830. https://doi.org/10.1002/adfm.202110830

[36] Zhang H, Li Y, Xu Y, Lu Z, Chen L, Huang L, Fan M (2016) Versatile fabrication of a superhydrophobic and ultralight cellulose-based aerogel for oil spillage clean-up. Phys Chem Chem Phys 18:28297–28306. https://doi.org/10.1039/C6CP04932J

[37] Zhang X, Wang H, Cai Z, Yan N, Liu M, Yu Y (2019) Highly compressible and hydrophobic anisotropic aerogels for selective oil/organic solvent adsorption. ACS Sustainable Chem Eng 7:332–340. https://doi.org/10.1021/acssuschemeng.8b03554

[38] He J, Zhao H, Li X, Su D, Zhang F, Ji H, Liu R (2018) Superelastic and superhydrophobic bacterial cellulose/silica aerogels with hierarchical cellular structure for oil adsorption and recovery. J Hazard Mater 346:199–207. https://doi.org/10.1016/j.jhazmat.2017.12.045

[39] Li J, Li J, Meng H, Xie S, Zhang B, Li L, Ma H, Zhang J, Yu M (2014) Ultra-light, compressible and fire-resistant graphene aerogel as a highly efficient and recyclable absorbent for organic liquids. J Mater Chem A 2:2934. https://doi.org/10.1039/c3ta14725h

[40] Mi H-Y, Jing X, Politowicz AL, Chen E, Huang H-X, Turng L-S (2018) Highly compressible ultra-light anisotropic cellulose/graphene aerogel fabricated by bidirectional freeze drying for selective oil adsorption. Carbon 132:199–209. https://doi.org/10.1016/j.carbon.2018.02.033

[41] Bi H, Xie X, Yin K, Zhou Y, Wan S, He L, Xu F, Banhart F, Sun L, Ruoff RS (2012) Spongy graphene as a highly efficient and recyclable sorbent for oils and organic solvents. Adv Funct Mater 22:4421–4425. https://doi.org/10.1002/adfm.201200888

[42] Liu T, Huang M, Li X, Wang C, Gui C-X, Yu Z-Z (2016) Highly compressible anisotropic graphene aerogels fabricated by directional freezing for efficient adsorption of organic liquids. Carbon 100:456–464. https://doi.org/10.1016/j.carbon.2016.01.038

[43] Zhou L, Xu Z (2020) Ultralight, highly compressible, hydrophobic and anisotropic lamellar carbon aerogels from graphene/polyvinyl alcohol/cellulose nanofiber aerogel as oil removing absorbents. J Hazardous Mater 388:121804. https://doi.org/10.1016/j.jhazmat.2019.121804

[44] Liu Y, Peng Y, Zhang T, Qiu F, Yuan D (2018) Superhydrophobic, ultralight and flexible biomass carbon aerogels derived from sisal fibers for highly efficient oil–water separation. Cellulose 25:3067–3078. https://doi.org/10.1007/s10570-018-1774-7

[45] Yao X, Yu W, Xu X, Chen F, Fu Q (2015) Amphiphilic, ultralight, and multifunctional graphene/nanofibrillated cellulose aerogel achieved by cation-induced gelation and chemical reduction. Nanoscale 7:3959–3964. https://doi.org/10.1039/C4NR07402E

[46] Wang C, Yang S, Ma Q, Jia X, Ma P-C (2017) Preparation of carbon nanotubes/graphene hybrid aerogel and its application for the adsorption of organic compounds. Carbon 118:765–771. https://doi.org/10.1016/j.carbon.2017.04.001

[47] Zhao X, Yao W, Gao W, Chen H, Gao C (2017) Wet-spun superelastic graphene aerogel millispheres with group effect. Adv Mater 29:1701482. https://doi.org/10.1002/adma.201701482

[48] Meng Y, Young TM, Liu P, Contescu CI, Huang B, Wang S (2015) Ultralight carbon aerogel from nanocellulose as a highly selective oil adsorption material. Cellulose 22:435–447. https://doi.org/10.1007/s10570-014-0519-5

[49] Li C, Jiang D, Liang H, Huo B, Liu C, Yang W, Liu J (2018) Superelastic and arbitrary-shaped graphene aerogels with sacrificial skeleton of melamine foam for varied applications. Adv Funct Mater 28:1704674. https://doi.org/10.1002/adfm.201704674